

Temperature dependence of Auger recombination in a multilayer narrow-band-gap superlattice

D.-J. Jang and Michael E. Flatté

Optical Science and Technology Center, Department of Physics and Astronomy, University of Iowa, Iowa City, Iowa 52242

C. H. Grein

Physics Department M/C 273, University of Illinois at Chicago, Chicago, Illinois 60607-7059

J. T. Olesberg, T. C. Hasenberg, and Thomas F. Boggess*

Optical Science and Technology Center, Department of Physics and Astronomy, University of Iowa, Iowa City, Iowa 52242

(Received 2 March 1998; revised manuscript received 29 June 1998)

Temperature and density-dependent Auger recombination rates are determined for a four-layer broken-gap superlattice designed for suppression of both Auger recombination and intersubband absorption. The structure is intended as the active region of both optically pumped and diode lasers operating in the midwave infrared. Auger recombination and intersubband absorption are thought to be among the primary factors contributing to high-threshold current densities in such devices. Ultrafast time-resolved photoluminescence upconversion was used to measure the Auger rates at lattice temperatures ranging from 50 to 300 K. Results are compared to calculated rates using the temperature-dependent, nonparabolic $\mathbf{K}\cdot\mathbf{p}$ band structure and momentum-dependent matrix elements. The calculations, which include umklapp processes in the superlattice growth direction, are in excellent agreement with the experimental results. Comparison of these results with those obtained in other mid-IR semiconductor structures verifies Auger suppression. The measured temperature-dependent Auger recombination rates, together with calculations of the gain, provide an upper bound for the characteristic temperature, $T_0 = 81$ K, for lasers utilizing this superlattice as an active region. [S0163-1829(98)01043-1]

INTRODUCTION

Midwave infrared (MWIR, 2–5 μm) diode lasers have been extensively studied recently due to their potential application to remote sensing, pollution monitoring, and infrared countermeasures. Significant progress has been made in the development of MWIR lasers, with much of the recent research in this spectral range focused on interband antimonide devices utilizing a variety of quantum-well and superlattice designs.¹ The realization of commercial devices operating at or near room temperature, i.e., compatible with thermoelectric cooling, has been elusive, however, particularly for the longer wavelength MWIR lasers. This is in part a consequence of Auger recombination in the narrow-band-gap active regions of these lasers. Auger recombination is a nonradiative, density-dependent process that typically increases strongly with decreasing band-gap energy and increasing temperature, thereby contributing to high threshold current densities and low maximum operating temperatures in interband MWIR lasers.

As a result of the negative effects of Auger recombination on interband MWIR semiconductor lasers and long-wavelength detectors, this process has received considerable attention as efforts have been made both to understand its impact on laser performance and to design strategies for its suppression. Theoretical efforts have^{2–4} focused on the use of band-structure engineering (1) to modify the band-edge density of states through strain and quantum confinement (a strategy similar to that used for near-IR semiconductors⁵) and (2) to arrange superlattice minigaps to eliminate final states for Auger transitions. An early success of this strategy was demonstrated by experiments using steady-state photo-

conductivity in longer wavelength ($E_g \sim 120\text{--}140$ meV) InAs/Ga_{1-x}In_xSb type-II superlattices.⁶ These authors showed that such narrow-band-gap superlattices (variations of which form the backbone of many current MWIR laser designs) can display Auger rates that are orders of magnitude smaller than those measured in Hg_{1-x}Cd_xTe samples with comparable band gaps. The measured results were found to be within a factor of 3 of theoretical results for this structure. Subsequent photoconductivity measurements at 77 and 300 K on an InAs_{0.85}Sb_{0.15}/In_{0.87}Al_{0.13}As_{0.91}Sb_{0.09} multiple quantum well [$E_g(5\text{ K}) = 343$ meV] illustrated the importance of final-state resonance for the Auger process.⁷ Auger rates for type-II antimonide quantum wells and superlattices with band gaps near 275 and 400 meV, respectively, have also been extracted from optically pumped lasers by employing measurements of the threshold pump intensity and calculations of the threshold carrier density.^{8,9} In both cases, Auger suppression relative to bulk materials was observed, and the temperature dependence of the Auger recombination was evaluated. Detailed theoretical calculations of the Auger rates were not presented in Refs. 7–9.

While the characterization of Auger recombination using photoconductivity and optically pumped laser performance have provided significant insight into this process in MWIR laser materials,^{7–9} both of these techniques possess limitations. For example, the photoconductivity measurements must be performed on samples grown on a semi-insulating substrate, leading to growth of the structures in Refs. 6 and 7 on lattice-mismatched GaAs substrates. In addition, these measurements require Ohmic contacts, and quantitative analysis using this technique relies on low-density measurements of the carrier mobilities. Both the photoconductivity

and the optically pumped laser results also require knowledge of the absorption coefficient at the optical excitation wavelength. Moreover, the analysis assumes steady-state excitation, which could be compromised by multimode operation of the excitation sources. The optically pumped laser results^{8,9} also can be influenced by factors related to the optical cavity. In addition, for these measurements, the Auger recombination cannot be uniquely isolated from other recombination processes.

Many of these limitations can be overcome using all-optical, device-independent, ultrafast techniques—approaches that have been widely applied in the visible and near IR, but less extensively in the MWIR due to both limited optical sources and limited interest in materials in this spectral region relative to the near IR. Such techniques offer the advantage of injecting a well-defined (and potentially well-calibrated) carrier density that can be probed from the time of injection through the time required for recombination to be complete. In addition, ultrafast optical techniques are contactless and do not require semi-insulating substrates. Through a combination of temporal resolution and variation of the optical excitation level, density-dependent recombination, such as Auger recombination, can be isolated readily from Shockley-Read-Hall recombination. We have recently reported¹⁰ subpicosecond, time-resolved, differential transmission measurements of Auger recombination at 300 K in a $(\text{Ga}_{0.75}\text{In}_{0.25}\text{Sb}/\text{InAs}/\text{Al}_{0.20}\text{Ga}_{0.80}\text{Sb})$ superlattice multiple quantum well (MQW) with a band-gap energy of 330 meV. This structure is similar to those employed successfully in a variety of MWIR diode lasers.¹¹ For these measurements the initial optically injected carrier density was determined from the optical excitation intensity and from the density dependence of the peak differential transmission measured. No significant Auger suppression was observed in this structure, a result that is consistent with subsequent detailed analysis of the band structure.⁴ We later used^{4,12} time-resolved differential transmission to measure the 300 K Auger rates in a 310 meV $\text{InAs}/\text{Ga}_{0.60}\text{In}_{0.40}\text{Sb}/\text{InAs}/\text{Al}_{0.30}\text{Ga}_{0.42}\text{In}_{0.28}\text{As}_{0.50}\text{Sb}_{0.50}$ superlattice, a structure similar to those successfully utilized¹³ in optically pumped lasers operating at 5.2 μm up to 185 K and at 3.7 μm up to 300 K. This structure was designed specifically for suppression of Auger recombination and intersubband absorption, and a factor of 4 reduction in the Auger rate was measured¹² relative to InAs, a wider band-gap bulk semiconductor. This four-layer superlattice will be the subject of the temperature-dependent measurements discussed below.

Here, we describe the application of an alternative ultrafast, all-optical technique, i.e., time-resolved photoluminescence (PL) upconversion,¹⁴ to measurements of the temperature dependence of Auger recombination in the aforementioned MWIR four-layer superlattice. Again, this technique is well established in the near IR but only sparsely applied in the MWIR.^{15–17} Advantages of this technique include the ability to readily extract the optically injected carrier density¹⁸ and the carrier temperature¹⁹ from time-resolved PL spectra. Knowledge of the carrier density is critical to any quantitative analysis of Auger recombination. Furthermore, measurement of the carrier temperature is crucial to the study of the temperature dependence of Auger recombination, since it is the carrier temperature that prima-

rily determines the Auger rate (although, as we show below, the temperature dependence of the band structure can also have measurable effects).

The temperature dependence of the Auger process is particularly relevant to diode laser design, since lasers designed for Auger suppression at one temperature may not be optimized at another,²⁰ and the temperature dependence in MWIR quantum wells and superlattices may not display the trends that one might anticipate from simple models.²¹ It is well known that in near-IR band-gap *bulk* materials the Auger rate increases strongly with increasing temperature.¹⁸ For near-IR band-gap *quantum wells*, however, the Auger rate has been found to depend only weakly on temperature, leading some investigators to conclude that phonon-assisted Auger recombination dominates in these structures.^{18,22} Others have concluded that band-to-band Auger recombination still dominates,²³ but electrostatic band-profile deformation influences the band-edge populations in a manner that decreases the temperature dependence of the Auger rate. The temperature dependence of Auger recombination in some *bulk* MWIR III-V semiconductors is more complicated than in near-IR materials. This is a consequence of the proximity of the spin-orbit split-off band energy Δ_0 to that of the fundamental gap E_g in narrow-band-gap semiconductors, such as InAs and related alloys. The split-off band can thereby provide resonant states for hole-hole Auger processes. Since the temperature dependences of E_g and Δ_0 are generally different, the Auger resonance energy may move relative to the band-gap energy, and, therefore, the Auger rate may increase or decrease with temperature.⁷ Similar arguments can be made with respect to subbands in MQW's and minibands in superlattices, potentially leading to unexpected temperature dependence to the recombination in such structures. For example, the Auger coefficient in a 275-meV band-gap $\text{InAs}/\text{Ga}_{0.69}\text{In}_{0.31}\text{Sb}/\text{InAs}/\text{AlSb}$ type-II MQW was found to increase with temperature modestly in a monotonic manner.⁸ On the other hand, the Auger coefficient was found⁹ to saturate with temperature in a 400 meV $\text{InAs}/\text{GaSb}/\text{Ga}_{0.75}\text{In}_{0.25}\text{Sb}/\text{GaSb}$ superlattice designed with a valence-band Auger resonance in the middle of a minigap. Furthermore, the Auger coefficient was found to actually decrease with temperature above ~ 180 K in a similar superlattice designed with a heavy-hole-1 to heavy-hole-3 Auger resonance.²⁴ Such widely varying results indicate the importance of understanding the temperature dependence of the Auger process in structures designed for MWIR lasers.

We will present both experimental and theoretical analyses of the temperature dependence of Auger recombination in a 310 meV, strain-balanced, broken-gap superlattice designed for suppression of Auger recombination and intersubband absorption at room temperature. Time-resolved MWIR PL upconversion was used to measure carrier recombination rates, and results are presented for lattice temperatures ranging from 50 to 300 K. We obtain excellent agreement between measured and calculated Auger rates, which are found to increase monotonically with lattice temperature and carrier density. The PL upconversion technique readily provides the carrier temperature, and we discuss the impact of hot carriers on our analysis. Finally, the temperature dependence of the Auger rate is used, together with estimates of threshold carrier density, to place an upper bound on the empirical

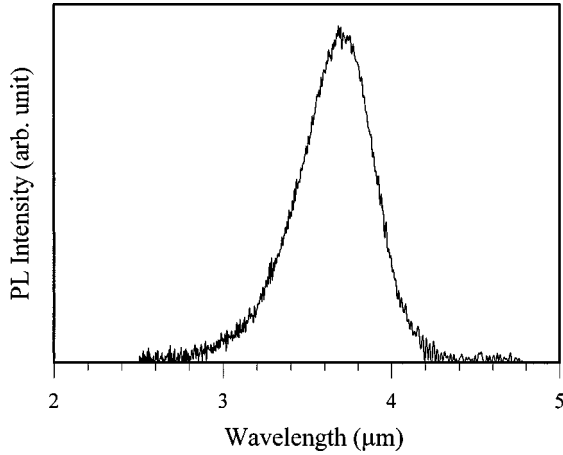


FIG. 1. Time-integrated photoluminescence at 300 K for continuous-wave excitation.

temperature parameter T_0 for lasers incorporating this structure as an active region.

SAMPLE STRUCTURE

The sample of interest for these studies was grown by molecular-beam epitaxy (MBE) on a nominally undoped GaSb substrate. It is comprised of 40 periods of an InAs (15 Å)/Ga_{0.60}In_{0.40}Sb (25 Å)/InAs (15 Å)/Al_{0.30}Ga_{0.42}In_{0.28}As_{0.50}Sb_{0.50} (39 Å) superlattice bounded by 1000 Å layers of Al_{0.30}Ga_{0.42}In_{0.28}As_{0.27}Sb_{0.73}. The structure is capped with 100 Å of GaSb to prevent oxidation of the Al containing quinary alloy. The superlattice is not intentionally doped and, although not determined specifically for this sample, background carrier densities in similar structures grown in the same MBE system are typically in the low 10^{15} cm⁻³ range. As shown in Fig. 1, under continuous wave excitation the sample exhibits strong room-temperature PL, from which a band gap of 310 meV (4 μm) is obtained.

The band-edge energies of the bulk constituents of a single period of the superlattice, shown in Fig. 2, illustrate

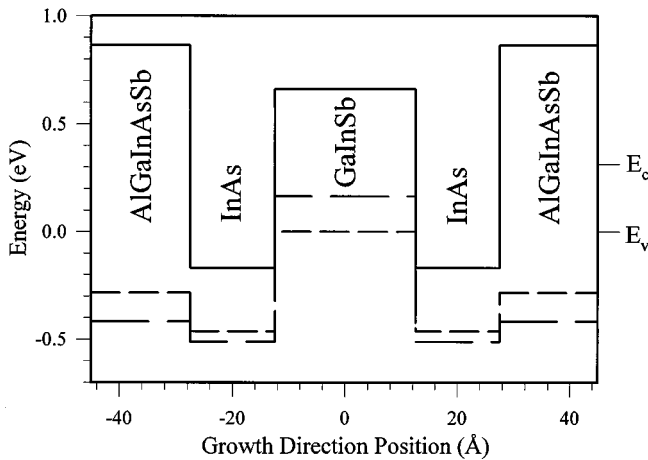


FIG. 2. Band-edge diagram for a single period of the narrow-band-gap superlattice. The solid, long-dashed, and short-dashed lines represent the conduction, heavy-hole, and light-hole bulk bands, respectively. The energy of the superlattice conduction- and valence-band edges are shown on the right side of the figure.

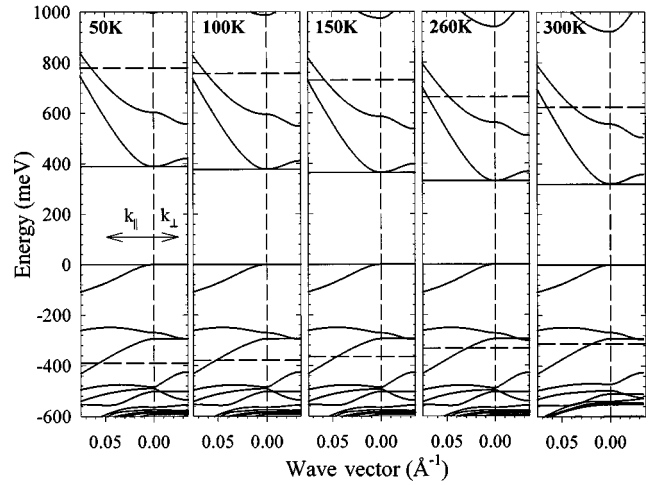


FIG. 3. Band structures along the in-plane direction (k_{\parallel}) and growth direction (k_{\perp}) for lattice temperatures of 50, 100, 150, 260, and 300 K. The band edges are indicated by the solid horizontal lines and the zone-center Auger resonance energies are indicated by the horizontal dashed lines.

the complicated type-II band alignments in this structure. The full nonparabolic band structure with momentum-dependent matrix elements is obtained from a superlattice $\mathbf{K}\cdot\mathbf{p}$ formalism similar to that applied previously to two-component superlattices^{2,25} but modified to allow for an arbitrary number of layers in a unit cell.⁴ The results of this calculation are shown in Fig. 3 for some of the lattice temperatures relevant to the experimental studies. Input parameters²⁶ to the calculation are limited to the energy levels, matrix elements, and effective masses of the bulk constituents, and valence-band offsets between layers. As seen in Fig. 3, the band-gap energy clearly decreases with increasing temperature, although the changes in dispersion of the various bands are rather subtle. Nevertheless, the temperature-dependent band gap results in a temperature dependence of the Auger and intersubband resonances. This is explicitly accounted for in our theoretical model of the Auger recombination and is borne out in our measurements of the temperature dependence of the Auger rates.

The superlattice has been designed to suppress Auger recombination and intersubband absorption at 300 K. This is accomplished through the reduction of the valence-band-edge density of states and through the elimination of states near zone center that are one band-gap energy above the lowest conduction subband edge and below the highest valence subband edge at a lattice temperature of 300 K. The design very effectively reduces intersubband absorption at 300 K for photon energies near that of the band gap.⁴ In addition, the light uppermost heavy-hole band leads to large differential gain in lasers based on such active regions.⁴ This in turn should result in low threshold current densities and, hence, low Auger rates at carrier densities appropriate for device operation. On the other hand, a detailed study of the band-structure dependence of the Auger rate in this structure indicates that the final-state optimization results in only about a factor of 2 suppression of the Auger rate at 300 K.²⁷ Considerably more suppression can be obtained through final-state optimization at lower temperatures, but a modification of the superlattice design is required.

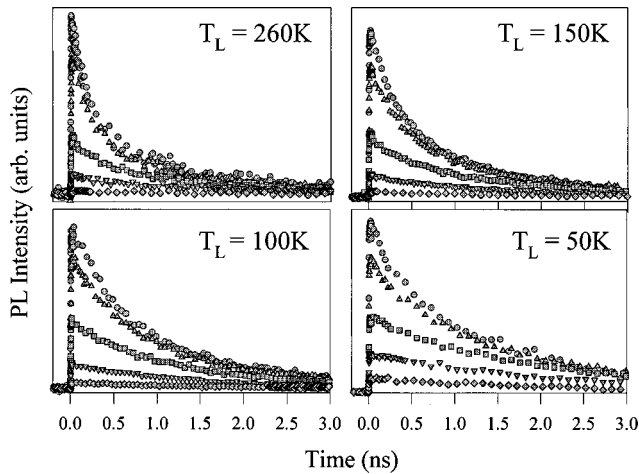


FIG. 4. Time-resolved photoluminescence measured near the band-gap energy for lattice temperatures of 50, 100, 150, and 260 K and initial carrier densities of (from the top) 1.7×10^{18} , 1.1×10^{18} , 5.7×10^{17} , 2.8×10^{17} , and $1.4 \times 10^{17} \text{ cm}^{-3}$.

EXPERIMENTAL RESULTS

Time-resolved PL upconversion was used to investigate the density and temperature dependence of the recombination in this superlattice. The MWIR PL, excited in the sample by an intense 140 fs, 843 nm pulse from a Kerr-lens mode-locked Ti:sapphire laser, was mixed with a portion of the same Ti:sapphire laser pulse in a potassium titanyl arsenate crystal oriented for phase-matched sum-frequency generation. The intensity of the measured upconverted signal is proportional to that of the PL emitted from the sample. Temporal resolution is obtained in the measurement by adjusting the relative delay between the pulse that excites the PL and the pulse that is used for the upconversion process. Spectral resolution is realized by adjusting the phase-matching angle and, simultaneously, a monochromator through which the upconverted signal passes. Details of the experimental setup have been described previously.¹⁶

PL decay curves for lattice temperatures of 50, 100, 150, 175, 200, 230, 260, and 300 K were measured for a range of initial carrier densities. Representative curves are shown in Fig. 4 for four lattice temperatures. The decay rate of the PL clearly increases both with increasing lattice temperature and increasing initial carrier density. We attribute the fast decay occurring within a few hundred picoseconds at high carrier densities to Auger recombination and the slower feature at longer delays to Shockley-Read-Hall recombination. These assertions are justified in the analysis discussed below.

The initial carrier densities, which are crucial in determining Auger rates, were calibrated by comparing selected experimental time-resolved PL spectra with those calculated based on the band structures shown in Fig. 3. For these measurements, the time delay between the pulse used to excite the sample and that used for the upconversion process was fixed at 10 ps and the entire PL spectrum was measured. The carrier temperature was extracted from the high-energy tail of the spectrum and used in calculations of the PL for a range of carrier densities. As illustrated in Fig. 5, the calculated PL spectra were then compared to the experimental spectra to yield the carrier density. Note that these results are plotted on a semilogarithmic scale to illustrate the exponential energy

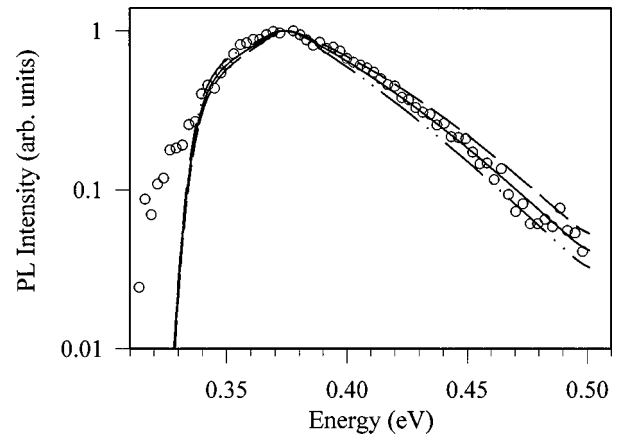


FIG. 5. Semilogarithmic plot of calculated (lines) and measured (circles) time-resolved (10 ps after excitation) photoluminescence for an excitation fluence of $8 \mu\text{J}/\text{cm}^2$, a lattice temperature of 260 K, and a carrier temperature of 300 K. Calculated PL for carrier densities of 4.5×10^{17} (dash-dot-dotted line), 5.7×10^{17} (solid line), and $7.0 \times 10^{17} \text{ cm}^{-3}$ (dashed line) are indicated.

dependence of the tail of the spectrum. The slope of this high-energy tail is primarily indicative of the carrier temperature, while for a reasonably cool distribution the overall width of the spectrum is largely controlled by the carrier density as a consequence of band filling. In fitting the spectrum, we fix the band-gap energy at the low-density value obtained from continuous wave PL (band-gap renormalization is insignificant at the densities of interest in this low-mass semiconductor), use the carrier temperature obtained from the high-energy portion of the spectrum, and then adjust only the carrier density to obtain a best fit to the data. The PL observed below the band edge is present at all densities indicating that it is a consequence of band tailing. These data are ignored in the fits. We assume in the calculations that within 10 ps after optical excitation the initially hot carriers diffuse across the thin superlattice and are uniformly distributed in the growth direction at the time of the measurement. Since the experimental arrangement ensures that only the emission from the central portion of the excited region of the sample is upconverted, transverse variations in the density are ignored. Shown in Fig. 5 are theoretical results for three values of the carrier density, illustrating that this procedure is sensitive to variations in density of approximately $\pm 20\%$. This process was repeated for various temperatures and excitation conditions. We conclude from this process and from knowledge of our optical excitation intensity that, over the range of our experimental conditions, essentially all of the incident photons transmitted through the semiconductor surface produce carriers that are confined to the superlattice, nominally independent of lattice temperature and excitation level. Hence, for this structure, the initial carrier density is readily determined from the incident photon flux.

DISCUSSION

The data in Fig. 4 are converted to density dependent rates $R(n)$ using

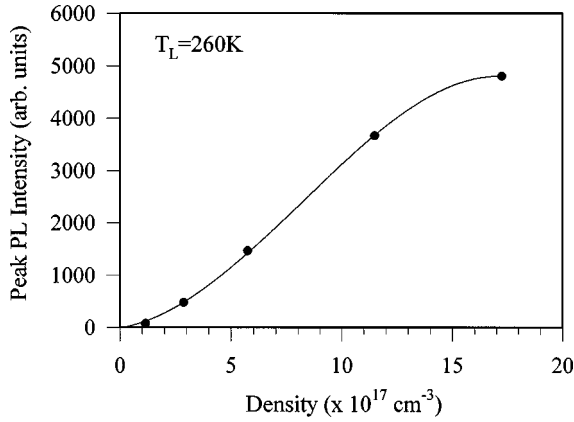


FIG. 6. Peak PL intensity as a function of carrier density for a lattice temperature of 260 K. The curve represents a smooth functional fit to the data from which the partial derivative dI_{PL}/dn is obtained and used in the evaluation of the recombination rate $R(n)$.

$$R(n) = \frac{1}{n} \frac{dn}{dt} = -\frac{1}{n} \frac{dn}{dI_{\text{PL}}} \frac{dI_{\text{PL}}}{dt},$$

where I_{PL} is the intensity of the PL and the derivatives are readily obtained from Fig. 4. Specifically, dI_{PL}/dt is obtained directly from Fig. 4 and dI_{PL}/dn is obtained from a functional fit to the peak PL signals measured at each excitation level. This procedure is illustrated in Fig. 6, where we show the fit and the normalized PL as a function of carrier density for the 260 K data, measured at a fixed time delay near the peak of the data shown in Fig. 4. $R(n)$ is interpreted as the sum of radiative and nonradiative rates. Photon reabsorption²⁸ is not considered here because of the small excitation beam size (50 μm , thin active region (0.375 μm), low band-edge absorption coefficient (approximately 2000 cm^{-1}), and relatively small radiative rate (never larger than 10% of the total recombination rate). Here, we are interested in primarily the nonradiative recombination rate. To obtain this for each density, we subtract from $R(n)$ the calculated radiative rate, a quantity that is readily determined from the band structure and matrix elements and is essentially insignificant relative to Shockley-Read-Hall and Auger recombination in this structure.

This procedure yields the nonradiative rates as a function of density as shown in Fig. 7 for the same lattice temperatures and initial carrier densities as depicted in Fig. 4. Note that the data shown in Fig. 7 originate, in essence, entirely from experiment, with theory invoked only to account for the minor effect of radiative recombination and to calibrate the initial carrier density. The intercepts in these plots yield the Shockley-Read-Hall rates, which correspond to lifetimes in all cases of about 2 ns. This value is within the 2–4 ns range typical of antimonide structures grown in this MBE system and is within a factor of 5 of the best MBE-grown antimonide structures studied in our laboratory. The specific origin of this density-independent recombination is not known, but may be associated with antisite defects in the quinary layers and/or interface states. Since the radiative rate has been removed from the results of Fig. 7, deviations from a zero slope are a consequence of Auger recombination. The data clearly illustrate an Auger rate that increases uniformly

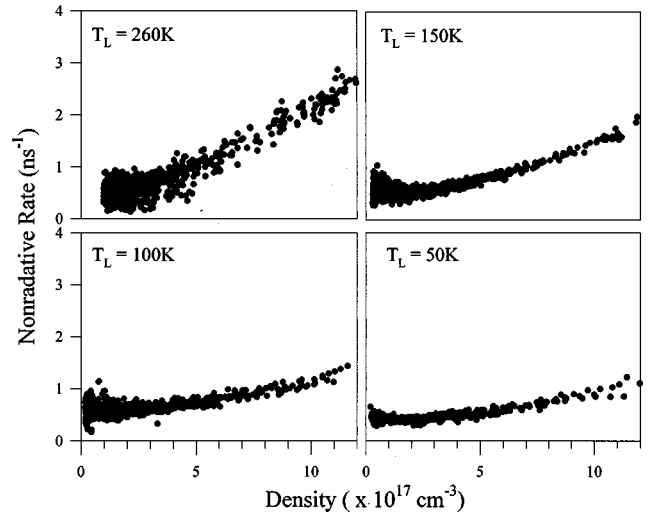


FIG. 7. Nonradiative recombination rates at lattice temperatures of 50, 100, 150, and 260 K obtained from the data in Fig. 4 using density calibrations such as that shown in Fig. 5 and the approach described in the text.

with both increasing carrier density and increasing temperature. We find that, over much of the density range of interest, the density dependence of the Auger rate is subquadratic with carrier density¹² as a consequence of degeneracy of both the conduction and valence bands. The effects of degeneracy have been confirmed through detailed investigations of the density dependence of the recombination, and the results will be discussed elsewhere.²⁹ The temperature dependence of the Auger process is seen more clearly in Fig. 8, where we plot the Auger rate as a function of lattice temperature for several different carrier densities.

The calculated direct band-to-band Auger rates are also shown in Fig. 8. These were obtained from Fermi golden-rule calculations based on the nonparabolic band structure with momentum-dependent matrix elements. Transition matrix elements are evaluated using a statically screened Coulomb interaction and first-order $\mathbf{K}\cdot\mathbf{p}$ perturbation theory for the wave-function overlaps. The implementation is similar

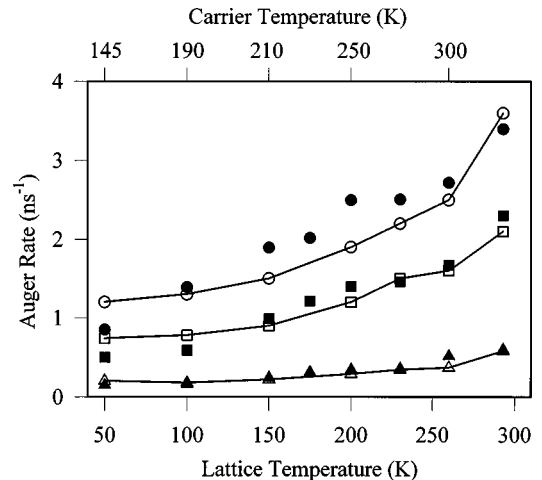


FIG. 8. Measured (filled symbols) and calculated (open connected symbols) Auger rates as a function of temperature for initial densities of 5×10^{17} (triangles), 10×10^{17} (squares), and $13 \times 10^{17} \text{ cm}^{-3}$ (circles).

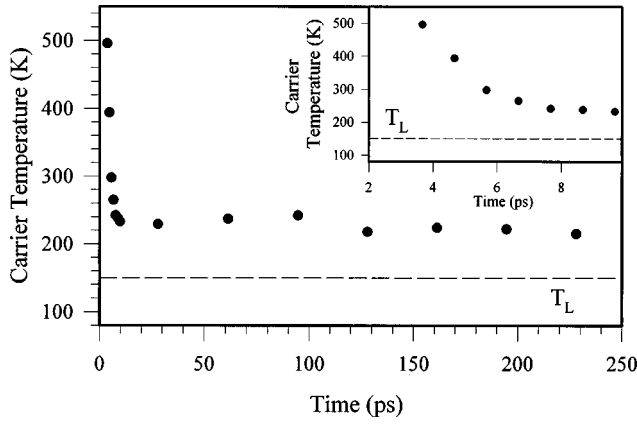


FIG. 9. Time dependence of the carrier temperature obtained from time-resolved photoluminescence for a lattice temperature of 150 K and an initial carrier density of $5.7 \times 10^{17} \text{ cm}^{-3}$. The inset shows an expanded view of the initial carrier cooling. The data indicate that the carrier distribution remains warmer than the lattice for hundreds of picoseconds.

to that reported previously,³⁰ but modified to include Umklapp processes in the growth direction.²⁹ This *intrinsic* phenomenon characterizes scattering processes that involve a reciprocal lattice vector.³¹ While these processes have little impact on Auger recombination in bulk narrow-gap semiconductors³² that have large reciprocal lattice vectors, they can play a significant role in superlattices. Zone folding in such structures greatly reduces the Brillouin-zone width in the growth direction (by more than an order of magnitude in our superlattice) making Umklapp processes more probable. Calculations indicate that these processes contribute approximately half of the total Auger rate in this structure. Umklapp processes involving a reciprocal lattice vector larger than $5(2\pi/D)$, where D is the superlattice period of 94 \AA , are negligible. We find that, *with no adjustable parameters*, the theory successfully predicts both the density dependence and the temperature dependence of the Auger process as well as the absolute rate. The latter, however, must be placed in context with the roughly 10% systematic and random error in the data and the 20% uncertainty in carrier density.

We have discussed the temperature dependence of the Auger process in terms of the lattice temperature. While the Auger process depends on the *lattice* temperature through the temperature dependence of the band structure, it will also depend on the occupation of the bands as determined by the *carrier* temperature. For our measurements, carriers are injected with roughly an electron volt of excess energy. Using time-resolved PL, we find that most of the cooling of the initially hot carrier distribution occurs within 10 ps, a time scale for which recombination is not significant. On the other hand, for high initial carrier densities we have observed somewhat elevated carrier temperatures that persist for many hundreds of picoseconds. This behavior is illustrated in Fig. 9, where we show the measured carrier temperature as a function of time after excitation for a lattice temperature of 150 K and an initial carrier density of $5.7 \times 10^{17} \text{ cm}^{-3}$. Although we have not completed a detailed analysis of this persistent heating, it may be due in part to Auger recombination itself, which supplies roughly the band-gap energy to the carrier distribution for each Auger event. Auger-induced

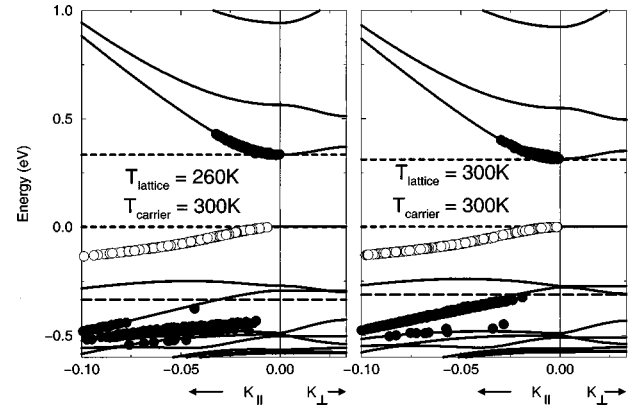


FIG. 10. Band structure of the superlattice indicating the band edge (short-dashed lines) and the valence-band zone-center Auger resonance energies (dashed lines) for lattice temperatures of 260 and 300 K and a carrier temperature of 300 K. The filled (open) circles represent electron (hole) states associated with $\sim 99\%$ of the hole Auger transitions at 260 K and 300 K for a carrier density of $5.7 \times 10^{17} \text{ cm}^{-3}$. The states are plotted as a function of in-plane momentum, $k_{\parallel} (\text{\AA}^{-1})$, only; hence, states not lying directly on a subband possess a growth direction momentum component $k_{\perp} (\text{\AA}^{-1})$.

carrier heating has been observed in wider band-gap structures with much lower Auger rates.³³ We use measurements such as those shown in Fig. 9 to obtain an average carrier temperature over time delays ranging from 10 ps to 1 ns for each of our Auger measurements. These temperatures, which are shown on the upper axis of Fig. 8, are used in the calculations of the Auger rates.

An important observation is that the average carrier temperature is essentially identical for the two highest lattice temperatures. On the other hand, the measured and calculated Auger rates are significantly different for these two lattice temperatures. This clearly indicates that the Auger rate has been modified strictly by the dependence of the band structure on the lattice temperature. Specifically, detailed analysis of the states involved in the Auger process reveal that at a lattice temperature of 260 K, most of the final hole states are in the fourth valence subband, whereas at 300 K they are in the third valence subband. This behavior, which arises from the slight decrease in E_g as the temperature is increased from 260 to 300 K, is illustrated in Fig. 10 where we show the electron (filled circles) and hole (open circles) states for $\sim 99\%$ of the Auger transitions for lattice temperatures of 260 and 300 K, and for a carrier temperature of 300 K. This figure clearly indicates that electrons near the Auger resonance in the valence bands (indicated by the dashed line) are more likely to participate in Auger transitions for a lattice temperature of 300 K compared to the case of a lattice temperature of 260 K. This implies that either a near-zone-center electron in the lowest conduction subband or a near-zone-center hole in the highest valence subband (or both) is more likely to participate in an Auger scattering process in the former case. Since the Fermi occupation factor is highest for near-zone-center particles, we therefore expect a significant increase in the Auger rate as the lattice temperature increases from 260 to 300 K, as calculated and observed.

The present calculation of the Auger rates does not in-

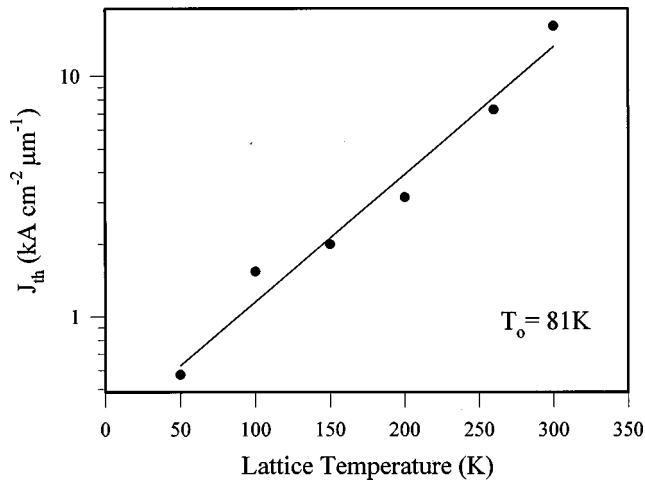


FIG. 11. Calculated threshold current density (filled circles) as a function of lattice temperature for a laser that uses the multilayer superlattice as an active region. In obtaining this result, a total loss of 100 cm^{-1} was assumed, the measured temperature-dependent recombination rates and the calculated threshold carrier densities were used. The slope of the resulting data, indicated by the solid line, yields $T_0 = 81 \text{ K}$, which represents an upper bound to the characteristic temperature.

clude phonon-assisted Auger recombination, which is expected to be rather insensitive to temperature variations. On the other hand, the calculation indicates that, in this structure, the rate associated with direct Auger processes increases modestly with temperature, a trend accurately reflected in the data. Although phonon-assisted transitions are certainly present, the agreement between the magnitude, density dependence, and temperature dependence of the measured rates and those calculated based purely on direct Auger transitions suggests that phonon-assisted Auger transitions do not significantly impact the nonradiative recombination in this structure.

The calculated band structure can be used, together with a band-filling model and calculations of the intersubband absorption, to obtain the temperature-dependent gain spectrum for this superlattice. This, combined with the measured Shockley-Read-Hall and temperature-dependent Auger rates, can be used to estimate the temperature-dependent threshold current density $J_{th}(T)$ per active layer width for lasers utilizing the superlattice for an active region. For an assumed total cavity loss of 100 cm^{-1} , we obtain a $J_{th}(300 \text{ K})$ of $16 \text{ kA cm}^{-2} \mu\text{m}^{-1}$. As shown in Fig. 11, a semilogarithmic plot of J_{th} as a function of temperature is well approximated by a straight line, and the inverse slope of $\ln(J_{th})$ yields the empirical characteristic temperature $T_0 = 81 \text{ K}$. We attribute this relatively high characteristic temperature to the suppression of Auger recombination and intersubband absorption in this structure throughout this temperature range. We note, however, that this T_0 is based solely on material properties. Since other temperature-dependent loss mechanisms may be present in an actual laser, this T_0 can be taken only as an upper limit (if Shockley-Read-Hall recombination remains small). Nevertheless, such a material parameter is a useful figure of merit for a laser gain medium.

SUMMARY AND CONCLUSIONS

In summary, we have measured and calculated Auger rates for a $4\text{-}\mu\text{m}$ band-gap type-II superlattice designed for suppression of Auger recombination and intersubband absorption at room temperature. The calculated Auger rates, which include superlattice Umklapp processes, were obtained using Fermi's golden rule for the transition rates and the full temperature-dependent, nonparabolic band structure. Umklapp processes, which provide roughly half of the total Auger rate, are found to be necessary to describe the experimental results. The experimental Auger rates were determined from time-resolved PL upconversion as a function of optically injected carrier density and lattice temperature. We find excellent agreement between measured and calculated rates for direct Auger transitions at all temperatures and carrier densities, which suggests that phonon-assisted Auger processes do not contribute significantly to the overall non-radiative recombination rate.

As discussed in more detail in Ref. 12, the 300 K Auger coefficient of $2.9 \times 10^{-27} \text{ cm}^6/\text{s}$ measured at low densities in the present structure is roughly a factor of 4 smaller than that of InAs,³⁴ even though the band gap of this bulk semiconductor is 50 meV wider. The coefficient is also nearly a factor of 3 smaller than that measured in a $(\text{Ga}_{0.75}\text{In}_{0.25}\text{Sb}/\text{InAs}/\text{Al}_{0.2}\text{Ga}_{0.8}\text{Sb})$ superlattice MQW with a 20-meV-wider band gap.¹⁰ On the other hand, the Auger coefficient measured at 300 K in our 310-meV band-gap superlattice is only $\sim 30\%$ smaller than that obtained in a 275-meV band-gap InAs/ $\text{Ga}_{0.69}\text{In}_{0.31}\text{Sb}/\text{InAs}/\text{AlSb}$ type-II MQW (Ref. 8). While such comparisons are necessary to attempt to determine the success of Auger suppression in a given structure, we caution that a simple comparison of coefficients is not adequate. We clearly observe saturation of the Auger coefficient in our structure¹² as a consequence of degeneracy. This saturation results in a high-density Auger rate that can be well below that expected assuming a simple quadratic carrier-density dependence for the rate. Saturation of the Auger coefficient was not observed in the structure studied in Ref. 10, and saturation *cannot* be quantified using the technique of Refs. 8 and 9. In addition, caution must be used in comparing Auger rates in various types of structures (bulk, quantum well, and superlattice) as carrier-density conventions vary. For example, in a superlattice it is reasonable to use a carrier density averaged over the superlattice period (as we have done in the present analysis), but three-dimensional densities in isolated quantum wells are usually determined based on the width of the well. In the latter case, sheet densities and two-dimensional Auger coefficients are often used. In either case, however, density variations along the growth direction will exist leading to a degree of ambiguity in the Auger coefficient.

We have used the measured temperature-dependent recombination rates and the calculated gain in the structure to extract an upper bound on the characteristic temperature of $T_0 = 81 \text{ K}$ for a laser based on this material. We presently have no direct experimental measure for T_0 for a laser utilizing this specific design as an active region. However, a T_0 of 37 K was obtained in a much longer wavelength ($5.2 \mu\text{m}$) optically pumped laser based on a similar superlattice design

and a 3.7 μm superlattice device has lased up to 300 K.¹³ A T_0 of 81 K for a MWIR laser, while lower than state-of-the-art near-IR lasers, would be exceptional if experimentally realizable for a MWIR laser. We emphasize again, however, that as long as the Shockley-Read-Hall recombination remains small this should be considered as an upper limit for T_0 , since other temperature-dependent loss mechanisms (e.g., carrier leakage) will exist in an actual device.

ACKNOWLEDGMENTS

This research was supported in part by the United States Air Force, Air Force Material Command, Air Force Research Laboratory, Kirtland AFB New Mexico 87117-5777 (Contract No. F29601-97-C-0041) and the National Science Foundation (Grant Nos. ECS-9406680 and ECS-9707799).

*Also at the Department of Electrical and Computer Engineering, University of Iowa, Iowa City, Iowa 52242. Electronic address: thomas-boggess@uiowa.edu

- ¹See, e.g., R. H. Miles and T. C. Hasenberg in *Antimonide Related Strain-Layer Heterostructures*, edited by M. O. Manasreh (Gordon and Breach, Amsterdam, 1998), pp. 433–460; J. I. Malin, C. L. Felix, J. R. Meyer, C. A. Hoffman, J. F. Pinto, C.-H. Lin, P. C. Chang, S. J. Murray, and S.-S. Pei, *Electron. Lett.* **32**, 1593 (1996); K. D. Moiseev, M. P. Mikhailova, O. G. Ershov, and Yu. P. Yakovlev, *Fiz. Tekh. Poluprovodn.* **30**, 399 (1996) [*Semiconductors* **30**, 223 (1996)]; H. K. Choi, G. W. Turner, M. J. Manfra, and M. K. Conners, *Appl. Phys. Lett.* **68**, 2936 (1996); S. R. Kurtz, R. M. Biefeld, A. A. Allerman, A. J. Howard, M. H. Crawford, and M. W. Pelczynski, *ibid.* **68**, 1332 (1996); D. Z. Garbuzov, R. U. Martinelli, H. Lee, P. K. York, L. A. DiMarco, M. G. Harvey, R. J. Matarese, S. Y. Narayan, and J. C. Connolly, *ibid.* **70**, 2931 (1997), and references therein.
- ²C. H. Grein, P. M. Young, and H. Ehrenreich, *Appl. Phys. Lett.* **61**, 2905 (1992).
- ³M. E. Flatté, C. H. Grein, H. Ehrenreich, R. H. Miles, and H. Cruz, *J. Appl. Phys.* **78**, 4552 (1995); C. H. Grein, P. M. Young, and H. Ehrenreich, *ibid.* **76**, 1940 (1994).
- ⁴Michael E. Flatté, J. T. Olesberg, S. A. Anson, Thomas F. Boggess, T. C. Hasenberg, R. H. Miles, and C. H. Grein, *Appl. Phys. Lett.* **70**, 3212 (1997).
- ⁵See, e.g., E. Yablonovich and E. O. Kane, *J. Lightwave Technol.* **6**, 1292 (1988); E. P. O'Reilly and A. R. Adams, *IEEE J. Quantum Electron.* **30**, 366 (1994).
- ⁶E. R. Youngdale, J. R. Meyer, C. A. Hoffman, F. J. Bartoli, C. H. Grein, P. M. Young, H. Ehrenreich, R. H. Miles, and D. H. Chow, *Appl. Phys. Lett.* **64**, 3160 (1994).
- ⁷J. R. Lindle, J. R. Meyer, C. A. Hoffman, F. J. Bartoli, G. W. Turner, and H. K. Choi, *Appl. Phys. Lett.* **67**, 3153 (1995).
- ⁸C. L. Felix, J. R. Meyer, I. Vurgaftman, C.-H. Lin, S. J. Murry, D. Zhang, and S.-S. Pei, *IEEE Photonics Technol. Lett.* **9**, 734 (1997).
- ⁹W. W. Bewley, I. Vurgaftman, C. L. Felix, J. R. Meyer, C.-H. Lin, D. Zhang, S. J. Murry, S.-S. Pei, L. R. Ram-Mohan, J. *Appl. Phys.* **83**, 2384 (1998).
- ¹⁰S. W. McCahon, S. A. Anson, D.-J. Jang, M. E. Flatté, Thomas F. Boggess, D. H. Chow, T. C. Hasenberg, and C. H. Grein, *Appl. Phys. Lett.* **68**, 2135 (1996).
- ¹¹T. C. Hasenberg, R. H. Miles, A. R. Kost, and L. West, *IEEE J. Quantum Electron.* **33**, 1403 (1997).
- ¹²J. T. Olesberg, Thomas F. Boggess, S. A. Anson, D.-J. Jang, M. E. Flatté, T. C. Hasenberg, and C. H. Grein, in *Infrared Applications of Semiconductors II*, edited by D. L. McDaniel, Jr., M. O. Manasreh, R. H. Miles, and Sivalingam Sivananthan, MRS Symposium Proceedings No. 484 (Materials Research Society, Pittsburgh, 1998), p. 83.

- ¹³M. E. Flatté, T. C. Hasenberg, J. T. Olesberg, S. A. Anson, T. F. Boggess, Chi Yan, and D. L. McDaniel, Jr., *Appl. Phys. Lett.* **71**, 3764 (1997).
- ¹⁴J. Shah, *IEEE J. Quantum Electron.* **24**, 276 (1988).
- ¹⁵D. von der Linde and R. Lambrich, *Phys. Rev. Lett.* **42**, 1090 (1979).
- ¹⁶D.-J. Jang, J. T. Olesberg, M. E. Flatté, Thomas F. Boggess, and T. C. Hasenberg, *Appl. Phys. Lett.* **70**, 1125 (1997).
- ¹⁷W. T. Cooley, Ph.D. thesis, Air Force Institute of Technology, 1997.
- ¹⁸See, e.g., S. Hauser, G. Fuchs, A. Hangleiter, K. Streubel, and W. T. Tsang, *Appl. Phys. Lett.* **56**, 913 (1990).
- ¹⁹See, e.g., Jagdeep Shah, in *Ultrafast Spectroscopy of Semiconductors and Semiconductor Nanostructures* (Springer, New York, 1996).
- ²⁰M. E. Flatté, C. H. Grein, and H. Ehrenreich, *Appl. Phys. Lett.* **72**, 1424 (1998).
- ²¹See, e.g., G. P. Agrawal and N. K. Dutta, *Semiconductor Lasers*, 2nd ed. (Van Nostrand, New York, 1993).
- ²²Yao Zau, Julian S. Osinski, Piotr Grodzinski, P. Daniel Dapkus, William C. Rideout, W. F. Sharfin, J. Schlafer, and F. D. Crawford, *IEEE J. Quantum Electron.* **29**, 1565 (1993); F. Fuchs, C. Schiedel, A. Hangleiter, V. Härle, and F. Scholz, *Appl. Phys. Lett.* **62**, 396 (1993).
- ²³Shunji Seki, Wayne W. Lui, and Kiyoyuki Yokoyama, *Appl. Phys. Lett.* **66**, 3093 (1995).
- ²⁴The authors indicate that this behavior may be an artifact of their analysis resulting from an overestimation of the threshold carrier density.
- ²⁵M. E. Flatté, P. M. Young, L.-H. Peng, and H. Ehrenreich, *Phys. Rev. B* **53**, 1963 (1996).
- ²⁶O. Madelung, in *Semiconductors, Group IV Elements and III-V Compounds*, edited by K.-H. Hellwege and O. Madelung, Landolt-Börnstein, New Series, Group III, Vol. 17, Pt. a (Springer-Verlag, Berlin, 1982).
- ²⁷Michael E. Flatté, J. T. Olesberg, and C. H. Grein, in *Infrared Applications of Semiconductors II* (Ref. 12), p. 71.
- ²⁸P. Asbeck, *J. Appl. Phys.* **48**, 820 (1977).
- ²⁹Michael E. Flatté, C. H. Grein, T. C. Hasenberg, S. A. Anson, D.-J. Jang, J. T. Olesberg, and Thomas F. Boggess, *Phys. Rev. B* (to be published).
- ³⁰C. H. Grein, P. M. Young, M. E. Flatté, and H. Ehrenreich, *J. Appl. Phys.* **78**, 7143 (1995).
- ³¹R. Peierls, *Ann. Phys. (Leipzig)* **12**, 154 (1932).
- ³²S. Brand and R. A. Abram, *J. Phys. C* **17**, 571 (1984).
- ³³See, e.g., H. Lobentzner, W. Stolz, J. Nagle, and K. Ploog, *Phys. Rev. B* **39**, 5234 (1989).
- ³⁴K. L. Vodopyanov, H. Graener, C. C. Phillips, and T. J. Tate, *Phys. Rev. B* **46**, 13 194 (1992).